ACS APPLIED MATERIALS & INTERFACES

Research Article

www.acsami.org

Colorimetric and Ratiometric Near-Infrared Fluorescent Cyanide Chemodosimeter Based on Phenazine Derivatives

Lin Yang,[†,§] Xin Li,[‡,§] Jiabao Yang,[†] Yi Qu,[†] and Jianli Hua*[,†]

[†]Laboratory for Advanced Materials and Institute of Fine Chemicals, East China University of Science and Technology, Shanghai 200237, People's Republic of China

[‡]Department of Theoretical Chemistry and Biology, School of Biotechnology, KTH Royal Institute of Technology, SE-10691 Stockholm, Sweden

Supporting Information

ABSTRACT: Two new near-infrared chemodosimeters for cyanide anion based on 5,10-dihexyl-5,10-dihydrophenazine were designed and synthesized. With dicyano-vinyl groups as the recognition site and electron-withdrawing groups on both sides, probe **1** exhibited an intramolecular charge transfer (ICT) absorption band at 545 nm and emission band at 730 nm, respectively, and thus showed an ICT block process and realized an "on−off" response after bilateral reaction with cyanide anions in CH_3CN. Probe **2** utilized an unreactive formyl group instead of one of the two reactive dicyano-vinyl groups as the electron-withdrawing component. Due to the unilateral recognition process the ICT of probe **2** was redirected and lead to a remarkably colorimetric and ratiometric near-infrared (NIR) fluorescent response for cyanine. Both probes provided high sensitivity and selectivity with apparent response signals which can be observed by naked eyes, even in the copresence of various other interference anions. Optical spectroscopic techniques, NMR titration measurements, and density functional theory calculations were conducted to rationalize the sensing mechanisms of these two probes.

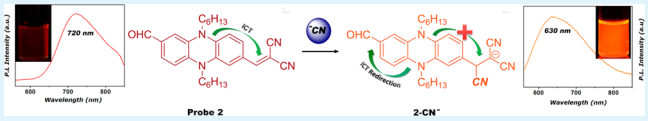

KEYWORDS: *colorimetry, near-infrared fluorescence, cyanide, phenazine derivatives, sensors, intramolecular charge transfer*

1. INTRODUCTION

The cyanide anion has been continuously of concern all over the world due to its high toxicity and widespread use in industrial processes such as acrylic fiber manufacturing, metallurgy, herbicide production, and silver or gold extraction.[1−3] Cyanide-containing substances, found in water, soil, polluted air, vehicle exhaust, and even cigarette burning gas, are extremely detrimental to human beings and most animals by causing lethal damage to their nervous systems.[4] Uptake of toxic cyanide could occur through absorption by lungs, exposure to skin, and also from contaminated food and polluted drinking water.[2−6] Nowadays, environmental pollution caused by cyanide is becoming severe due to the aggravation of the industrialization process; convenient and efficient detection of cyanide anions is called for in the battle against such pollution.[7]

Many different methods have been developed for the detection of cyanide anions. Traditional methods including electrochemical analysis and ion chromatography require long-time procedures and the involvement of intelligent instruments,[8] whereas chemical sensors provide another approach which is simple, inexpensive, and rapid in real-time monitoring.[2] The sensing process is often accompanied by changes in absorption or fluorescence spectra that can be precisely monitored and sometimes detected by the naked eye.

The cyanide anion is characterized by its nucleophilicity, Lewis basicity,[9−11] and ability of forming strong hydrogen bonds in aqueous solution,[2,12] based on which a variety of sensors have been reported during recent years.[13−16] Compared to hydrogen bond or Lewis basicity based sensors, chemodosimeters take advantage of the unique nucleophilicity of cyanide to realize recognition through the bond-formation reaction between the probing molecule and cyanide anions.[12] The functioning mechanisms of chemodosimeters, particularly the change of optical spectra upon recognition, rely on the structure of π-conjugation and reactive subunit. Hitherto, coumarin,[17−25] calix[4]pyrrole,[26,27] BODIPY,[28−30] oxazine,[31,32] hemicyanine, and cyanine[33] moieties have been employed as the π-conjugation framework, and the electrophilic C═C[34] double bond and C—B[28,35−37] single bond have been adopted as the reactive subunit.

Several chemodosimeters containing dicyano-vinyl electrophilic C═C double bonds as the reactive subunit have been reported.[34,37] However, few of them displayed synchronous colorimetric and ratiometric responses in the near-infrared (NIR) region. Ratio signals can be employed to rectify the systematic error introduced by interference of environmental conditions, solution concentrations, and background disturbances compared to a monosignal system.[38−41] NIR fluorescence response, ascribed to the emission wavelength of 650−900 nm, is highly desirable in bioimaging for deeper penetration into

Received: November 5, 2012
Accepted: January 28, 2013
Published: January 28, 2013

tissue with weak scattering, low damage to living cells, and negligible autofluorescence background signal.[42,43]

In this work, we report the design, synthesis, and sensing performance of new cyanide probes **1** and **2** (Chart 1) based on

Chart 1. Molecular Structures of Probes 1 and 2

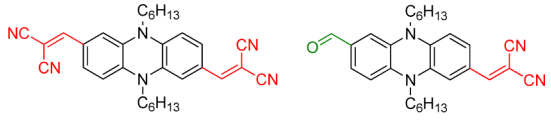

phenazine structure with a dicyano-vinyl group as the reaction site. Although phenazine and its derivatives have been extensively studied over the past ten years due to their biological and chemical importance,[44−46] to the best of our knowledge, this is the first cyanide sensor based on phenazine π-conjugated skeleton.

2. EXPERIMENTAL SECTION

2.1. Instrumentation and Materials. ^{1}H NMR and ^{13}C NMR spectra were recorded on a Bruker AM 400 MHz spectrometer with tetramethyl silane (TMS) as an internal reference. Absorption spectra were measured on a Varian Cary 500 UV−vis spectraphotometer. Fluorescence spectra were measured on a Horiba Fluoromax-4 Fluorescence spectrometer. Mass spectra were recorded with a Waters Micromass LCT mass spectrometer.

N,*N*-Dimethylformamide (DMF) was refluxed with calcium hydride and distilled before use. All other reagents and reactants including phenazine were purchased as commercial products from Aldrich and used as received without further purification.

2.2. ^{1}H NMR Titration. ^{1}H NMR titration spectra were carried out via the addition of 0−1.0 and 0−2.0 equiv of cyanide anion to probe **1** in $CDCl_3$ and **2** DMSO-d_6, respectively, at room temperature.

2.3. Theoretical Calculations. All theoretical calculations were carried out by using the Gaussian 09 program package.[47] Geometries of the compounds were optimized by using density functional theory (DFT) calculations at the B3LYP/6-31G* level of theory,[48,49] and then, time-dependent density functional theory (TDDFT) calculations were carried out with solvent effects of acetonitrile taken into account by the polarizable continuum model (PCM).[50] The PBE0 functional[51] was used together with the 6-31G* basis set in TDDFT calculations as suggested by Leang et al.[52] For each compound, geometry of the first singlet excited state (S_1) was also optimized by TDDFT calculations, from which the electronic transition energy for fluorescent process can be obtained.

2.4. Selectivity Measurements. The changes in the absorption and fluorescence spectra (both in CH_3CN, 10 μM at 25 °C) caused by CN^- (20 μM) and miscellaneous interference anions (200 μM) including F^-, Cl^-, Br^-, I^-, PO_4^{3-}, CO_3^{2-}, SO_4^{2-}, NO_3^-, SCN^-, AcO^-, HSO_3^-, NO_2^-, and HCO_3^- with their Na^+ or K^+ salts in water solutions were recorded.

2.5. Synthesis of Probes 1 and 2. *2.5.1. Synthesis of 5,10-Dihydrophenazine (**6**).* Phenazine (2.84 g, 15.8 mmol) was dissolved in 70 mL ethanol. Under argon atmosphere, the mixture was heated to refluxing, then, added $Na_2S_2O_4$ (28.4 g, 0.16 mol) dissolved in water. The color of the mixture changed immediately to blue; then, a large amount of white precipitation came out. About 1 h later, heating of the reaction mixture was stopped and it was cooled to room temperature then filtered, washed with water, and dried in vacuo. The light green solid was collected and weighed 3.82 g. Because of its instability in air,[46] it was not characterized by NMR spectra and was quickly put into the next step reaction.

*2.5.2. Synthesis of 5,10-Dihexyl-5,10-dihydrophenazine (**7**).* A mixture of sodium hydroxide (2.4 g, 0.06 mol), tetrabutylammonium bromide (0.4 g, 1.2 mmol), and **6** (3.82 g, 0.02 mol) crude product was dissolved in 70 mL DMSO and 1.5 mL H_2O. After stirring for 5 min, hexyl bromide (5 mL, 0.035 mol) was added. The mixture was then heated to 40 °C, and stirring was continued for 3.5 h. After cooling to room temperature, the reaction mixture was poured into water, filtered, and dried in vacuo. The crude product was purified by neutral aluminum oxide chromatography, using petroleum ether as an eluent to isolate pure compound **7** (3.9 g, 69%) as a light green crystal. ^{1}H NMR (400 MHz, C_6D_6), δ (ppm): 6.69−6.63 (m, 4H), 6.28−6.21 (m, 4H), 3.18−3.12 (m, 4H), 1.54−1.41 (m, 4H), 1.24−1.14 (m, 4H), 1.12−1.03 (m, 8H), 0.86−0.83 (t, J = 7.2 Hz, 6H). ^{13}C NMR (100 MHz, C_6D_6), δ (ppm): 137.44, 121.12, 110.90, 45.32, 31.66, 26.71, 24.54, 22.92, 14.13. HRMS (ESI, m/z) $[M]^+$ calcd for $C_{24}H_{34}N_2$: 350.2722. Found: 350.2719.

*2.5.3. Synthesis of 5,10-Dihexyl-5,10-dihydrophenazine-2-carbaldehyde (**8**).* **7** (1.4 g, 3.9 mmol) was dissolved in 14 mL DMF and stirred under an argon atmosphere. The reactor was kept in ice bath, and phosphorus oxychloride (1 mL) was slowly added into the solution. The resulting mixture was then stirring in 40 °C for 7 h, and then, cooled to room temperature. After pouring into ice water and stirring until the ice melted, sodium hydroxide solution was added dropwise until the pH value of the mixture was adjusted to 7.0. The color of the mixture turned from dark green into red orange, and the precipitation was filtered and dried in vacuo. The crude product was purified by silica gel chromatography using petroleum/CH_2Cl_2 (2:1) as an eluent to isolate pure compound **8** (443 mg, 30%). ^{1}H NMR (400 MHz, C_6D_6) δ (ppm): 9.66 (s, 1H), 6.90 (s, 1H), 6.78 (s, 1H), 6.58 (s, 2H), 6.14 (d, J = 6.7 Hz, 2H), 5.93 (d, J = 7.7 Hz, 1H), 3.06−2.96 (m, 4H), 1.50−1.38 (m, 2H), 1.37−1.27 (m, 2H), 1.24−1.13 (m, 4H), 1.11−1.01 (m, 8H), 0.90−0.81 (m, 6H). ^{13}C NMR (100 MHz, C_6D_6) δ (ppm): 188.95, 143.16, 137.51, 136.57, 135.09, 131.09, 128.69, 122.71, 121.14, 111.65, 111.26, 109.21, 107.07, 45.41, 45.17, 31.51, 26.52, 24.44, 24.00, 22.88, 14.10. HRMS (ESI, m/z) $[M]^+$ calcd for $C_{25}H_{34}N_2O$: 378.2671. Found: 378.2673.

*2.5.4. Synthesis of 5,10-Dihexyl-5,10-dihydrophenazine-2,7-dicarbaldehyde (**9**).* The synthesis route of compound **9** is similar to compound **8**, and the only differences are the reaction temperature which was promoted to 90 °C and the stirring time which was lasted 12 h. The crude product was purified by silica gel chromatography using petroleum/CH_2Cl_2 (1:1) as an eluent. The isolated pure compound **9** was orange in color (967 mg, 61%). ^{1}H NMR (400 MHz, $CDCl_3$) δ (ppm): 9.60 (s, 2H), 7.11 (d, J = 7.8 Hz, 2H), 6.71 (s, 2H), 6.26 (d, J = 8.1 Hz, 2H), 3.43 (t, J = 8.0 Hz, 4H), 1.69−1.61 (m, 4H), 1.48−1.35 (m, 12H), 0.94 (t, J = 7.0 Hz, 6H). ^{13}C NMR (101 MHz, $CDCl_3$) δ (ppm): 189.81, 142.52, 135.18, 130.17, 109.77, 108.25, 45.77, 31.44, 26.47, 25.62, 24.15, 22.67, 14.01.

*2.5.5. Synthesis of 2,2′-((5,10-Dihexyl-5,10-dihydro-phenazine-2,7-diyl)bis(methanylydiene))dimalononitrile (**1**).* The mixture of excess malononitrile, ammonium acetate (150 mg) and **9** (406 mg, 1.0 mmol) was dissolved in 24 mL acetic acid and refluxed under an argon atmosphere for 6 h. After cooling to room temperature, the mixture was poured into water, and the precipitation was filtered and dried. The crude product was purified by silica gel chromatography using petroleum/CH_2Cl_2 as eluent. The pure product was obtained (306 mg, 60%). ^{1}H NMR (400 MHz, $CDCl_3$), δ (ppm): 7.31 (s, 2H), 7.19 (d, J = 1.6 Hz, 2H), 6.95 (dd, J_1 = 8.5 Hz, J_2 = 1.8 Hz, 2H), 6.27 (d, J = 8.5 Hz, 2H), 3.43 (t, J = 8.3 Hz, 4H), 1.70−1.60 (m, 4H), 1.47−1.41 (m, 4H), 1.40−1.33 (m, 8H), 0.92 (t, J = 7.0 Hz, 6H). ^{13}C NMR (101 MHz, $CDCl_3$), δ (ppm): 156.81, 142.76, 134.27, 133.15, 124.81, 115.10, 114.36, 110.46, 109.24, 75.08, 46.34, 31.49, 26.20, 24.46, 22.60, 14.00. HRMS (ESI, m/z) $[M + H]^+$ calcd for $C_{32}H_{35}N_6$: 503.2923. Found: 503.2925. Elemental analysis (%, found/calcd): C, 76.31/76.46; H, 6.90/6.82; N, 16.81/16.72.

*2.5.6. Synthesis of 2-((7-Formyl-5,10-dihexyl-5,10-dihydrophenazin-2-yl)methylene) Malononitrile (**2**).* A mixture of malononitrile (66 mg, 1 mmol), ammonium acetate (75 mg), and **9** (406 mg, 1 mmol) was dissolved in 12 mL acetic acid and refluxed under an argon atmosphere for 6 h. After cooling to room temperature, the mixture was poured into water, and the precipitation was filtered and dried. The crude product was purified by silica gel chromatography using petroleum/CH_2Cl_2 as eluent. The pure product was dark green in color (136 mg, 30%). ^{1}H NMR (400 MHz, DMSO-d_6) δ (ppm): 9.61

Scheme 1. Synthesis Procedures of Probes 1 and 2[a]

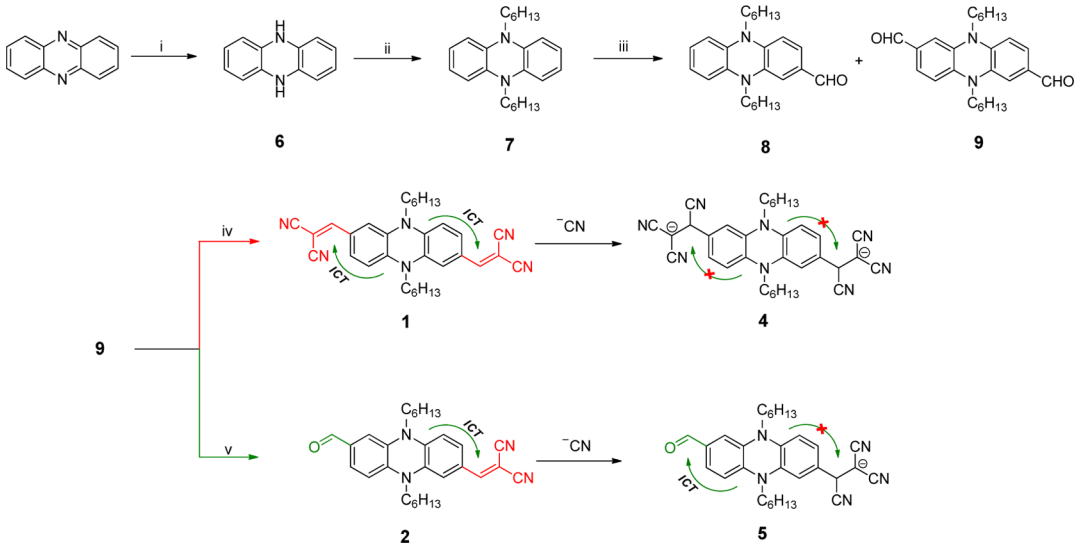

[a](i) $Na_2S_2O_4$, EtOH, H_2O, 80 °C, 2 h; (ii) hexyl bromide, sodium hydroxide, TBAB, DMSO, H_2O, rt, 3.5 h; (iii) phosphorus oxychloride, DMF, ice bath to 40 °C, 7 h, or 90 °C, 12 h; (iv) excess malononitrile, ammonium acetate, acetic acid, reflux, 6 h; (v) the same procedure as iv.

(s, 1H), 7.97 (s, 1H), 7.26 (dd, J_1 = 8.2 Hz, J_2 = 1.3 Hz, 1H), 7.20 (dd, J_1 = 8.6 Hz, J_2 = 1.6 Hz, 1H), 6.99 (d, J = 1.6 Hz, 1H), 6.77 (d, J = 1.3 Hz, 1H), 6.53 (d, J = 8.5 Hz, 2H), 3.53−3.47 (t, 2H), 3.41−3.35 (t, 2H), 1.57−1.47 (m, 4H), 1.44−1.36 (m, 4H), 1.36−1.29 (m, 8H), 0.95−0.85 (m, 6H). ^{13}C NMR (101 MHz, DMSO-d_6) δ (ppm): 190.07, 158.00, 142.75, 141.36, 134.19, 133.32, 132.73, 129.90, 129.55, 124.61, 115.72, 114.98, 110.87, 110.71, 109.63, 108.63, 106.40, 71.57, 54.89, 45.31, 44.57, 30.99, 30.82, 25.54, 23.75, 23.57, 22.13, 22.09, 13.85. HRMS (ESI, m/z) $[M + H]^+$ calcd for $C_{29}H_{35}N_4O$: 455.2811. Found: 455.2815. Elemental analysis (%, found/calcd): C, 76.55/76.62; H, 7.62/7.54; N, 12.41/12.32.

3. RESULTS AND DISCUSSION

3.1. Molecular Design and Synthesis. Our idea is to make use of the nucleophilic addition reaction of CN^- with a dicyano-vinyl group as the strategy for the design of a probe to track CN^- levels. For this purpose, probes **1** and **2** were designed and synthesized (Chart 1). **1** contains two dicyano-vinyl acceptor groups which are connected by a dihydrophenazine donor moiety. Differing from two same acceptors of probe **1**, probe **2** has a formyl group and just one dicyano-vinyl group as receptor. As shown in Scheme 1, the presence of the two hexyl groups changed the initial electron-deficient phenazine group into an electron-rich conjugation bridge. After attachment of electron-withdrawing groups like two dicyano-vinyl groups (**1**) or formyl and dicyano-vinyl groups (**2**) onto the 3- and 8-carbon position, stabilized intramolecular charge transfer (ICT) systems with acceptor−donor−acceptor (A−D−A) configurations were promoted. The electron-withdrawing nature of dicyano-vinyl group can be modulated by cyanide anion, which interrupts the π-conjugation through nucleophilic addition reaction.[53]

The role of dicyano-vinyl in the sensing mechanism was monitored by a comparison among the fluorescence emission spectra of probe **1**, probe **2**, and their precedent product compound **8** (Scheme 1) in their CH_3CN solutions (Figure 1). Before addition of a cyanide anion, probes **1** and **2** displayed NIR emission bands at 730 and 720 nm, respectively, while compound **8** showed a maximum emission band at 620 nm (Figure 1). To our knowledge, these emission bands arose from

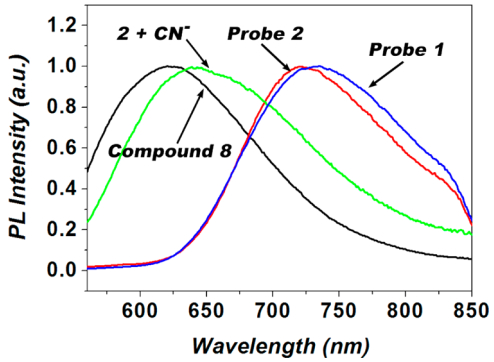

Figure 1. Comparison of normalized fluorescence emission spectra of **1**, **2**, and **8** in their CH_3CN solution before and after the addition of excess equivalent of cyanide anion in water. The emission spectrum of probe **1** after addition of cyanide does not appear because of its negligible intensities.

the ICT involved electron-donor group (dihydrophenazine core) and electron-withdrawing groups (formyl and dicyano-vinyl groups). An intriguing shift in emission spectrum was observed when an excess amount of cyanide was added into the CH_3CN solution of probe **2** (Figure 1). The NIR emission peak of probe **2** disappeared while a new arising emission band at around 630 nm particularly resembled the maximum emission wavelength of compound **8**, in which only a formyl group is attached to the 3-position of dihydrophenazine group.

Nucleophilic attack by equivalent cyanide anion was expected to occur toward the electrophilic C of the C=C double bond (as shown in Scheme 1, Figures 8 and 9). During the addition reaction, the electron-withdrawing dicyano-vinyl group was expected to be transformed into an anionic electron-rich group due to the destruction of the C=C double bond and the simultaneously emerged negative charge. In probe **1** both dicyano-vinyl acceptors became donors after cyanide addition; however, in probe **2**, a new acceptor−donor−donor (A−D−D) system of **5** (Scheme 1) would take effect and redirect the direction of ICT. This redirection effect in ICT resulted in a new emission band at 630 nm (Figure 1) making it possible to

construct an NIR ratiometric sensor based on the platform of probe **2**. Inspection into the phenomena and mechanisms of the sensing process was taken and described below.

The synthesis of probes **1** and **2** started from reduction and alkylation of the phenazine skeleton group (Scheme 1). And then formylation of the side phenyl rings was conducted through Vilsmeier−Haack reaction. After Knoevenagel reaction with equivalent or excess malononitrile, the desirable products were obtained, respectively. The structures were confirmed by ^{1}H and ^{13}C NMR spectroscopy and MS-ESI analysis. The details of synthesis and the structural identification spectra were formulated in the Supporting Information.

3.2. Optical Response of Probe 1 toward Cyanide Anion. We first explored the optical response of probe **1** by monitoring the changes in the absorption and fluorescence intensity spectra in acetonitrile solution upon gradual addition of aqueous CN^-. Probe **1** (10 μM in CH_3CN) was purple and exhibited main absorption bands centering at 545 and 372 nm. Upon addition of 0−0.4 equiv of cyanide anion, the absorption band at 545 nm decreased and bathochromically shifted to 600 nm with an isosbestic point at 612 nm, while the absorbance at 372 nm displayed a hypsochromic shift to 350 nm (Figure 2a). As titration continued, the absorption intensity at 600 nm decreased without shift until the saturation point was reached after addition of 2.8 equiv of cyanide anion (Figure 2b). Meanwhile, another shifted absorption peak at 350 nm also decreased and exhibited a further bathochromic shift of 15 nm (Figure 2b).

The particular characteristic of probe **1** is the two-step reaction with CN^- anion. One of the two dicyano-vinyl groups was first attacked by cyanide anion and transformed into a negatively charged electron-rich tricyano-ethyl group. The ICT absorption band showed bathochromic shift from 545 to 600 nm, for the ICT originally from phenazine core to dicyano-vinyl groups was changed into a monolateral electron transfer process from the phenazine group to the remained dicyano-vinyl group. After addition of nearly 1.0 equiv of cyanide, the color of the solution changed from its original purple to light blue, which could be observed by the naked eye (Figure 2c inset). As the addition continued, more equivalents of cyanide engaged in the reaction and started to attack the other dicyano-vinyl unsaturated double bond. The absorption band at 600 nm decreased and finally disappeared after 2.8 equiv of cyanide was added. The absorption band arising from the monolateral ICT system disappeared, and the solvent obviously faded to being almost colorless which could also be detected by the naked eye (Figure 2c inset).

The absorption intensity plots and Benesi−Hildebrand plots of absorbance at 545 and 612 nm upon addition of cyanide anion are shown in Figure 3, respectively. The linear correlation (blue dashed line) between $1/\Delta A_{545}$ and $1/[CN^-]$ at low concentration of CN^- (no larger than 0.15 equiv) confirmed the 1:1 stoichiometric reaction between **1** and CN^-. When $[CN^-]$ is larger than 0.15 equiv, the slope of the linear correlation changed, indicating the formation of $[CN-\mathbf{1}-CN]^{2-}$. This is also reflected by the absorbance at the isosbestic point of **1** and $[\mathbf{1}-CN]^-$ (612 nm), which remained almost constant at low concentration of CN^- and started to decrease accompanied by the formation of $[CN-\mathbf{1}-CN]^{2-}$.

Interestingly, probe **1** shows different emission spectra upon excitation at 540 and 400 nm. As shown in Figure 4, when the excitation wavelength was set up at 540 nm, an intense NIR emission band at around 730 nm was detected and sharply

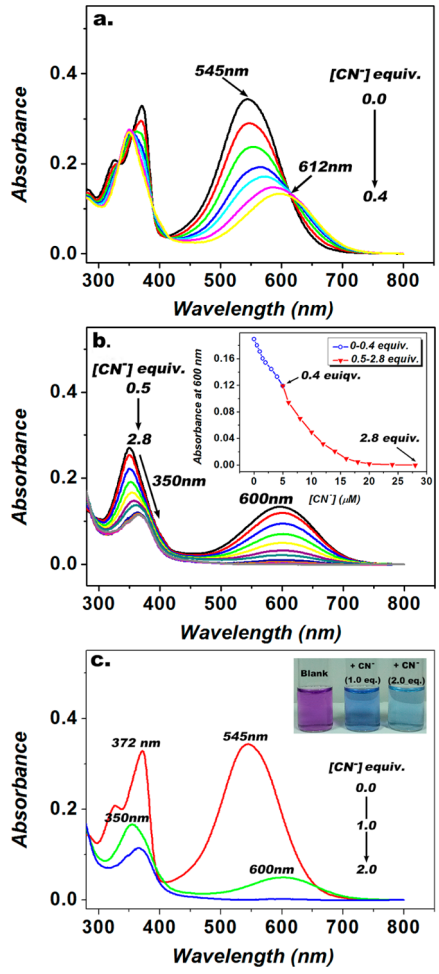

Figure 2. (a) Absorbance spectra of **1** in CH_3CN (10 μM) upon addition of 0−0.4 equiv of aqueous cyanide. (b) Absorbance spectra of probe **1** in CH_3CN (10 μM) upon addition of 0.5−2.8 equiv of aqueous cyanide anion. (inset) Plot of absorbance change at 600 nm. (c) Absorbance spectra of probe **1** in CH_3CN (10 μM) upon addition of 0, 1.0, and 2.0 equiv of aqueous cyanide anion. (inset) Concomitant color change of probe **1** (10 μM in CH_3CN) in the absence and presence of cyanide anion under a daylight lamp from purple to almost colorless.

decreased upon addition of cyanide. Particularly, when the added equivalent of cyanide reached above 0.4, the decreasing fluorescence intensity at 730 nm quickly reached the saturated point and stayed unchanged during the continued titration process (Figure 4, inset), showing an ideal linear dependence before the saturation point at about 0.4 equiv of cyanide anion (Supporting Information Figure S18).

Furthermore, when excited at 400 nm, a broadened emission band at around 600 nm was detected, which sharply decreased upon addition of cyanide (Figure 5a). Similarly, after addition of 0.4 equiv of cyanide, the intensity of the emission band at 600 nm reached its minimum which is in keeping with the saturation point upon excitation at 540 nm. As the addition of cyanide went on, a new emission band at 500 nm emerged (Figure 5b). The saturated point was reached after addition of 2.8 equiv of cyanide, which is in good agreement with the saturation point in the variation of absorption spectra (Figure 2b inset).

The detection limit of probe **1** for cyanide anion was measured using fluorescence intensity plot against CN^-

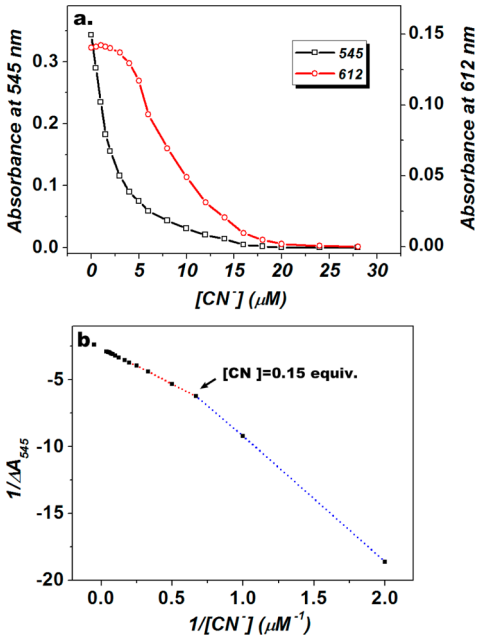

Figure 3. (a) Change of absorbance of **1** (10 μM) in CH_3CN at 545 nm (black line) and 612 nm (red line) upon addition of CN^- (0–2.8 equiv). (b) Benesi–Hildebrand plot of absorbance at 545 nm.

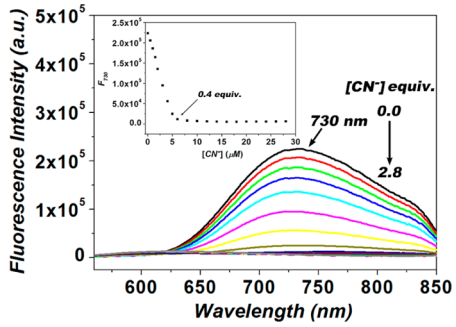

Figure 4. Fluorescence emission spectra of **1** (10 μM) in CH_3CN with titration of CN^- (0–28 μM) in water, λ_{ex} = 540 nm. (inset) Fluorescence response at 730 nm as a function of CN^- concentration (0–28 μM).

concentrations ranging from 0.0 to 4.0 μM, which provided a good linear correlation and a remarkable detection limit[54] of 5.77 × 10^{-8} M (see Figure S18 in page S13, Supporting Information). Thus, the acutely reduced NIR fluorescent intensity provided an explicit signal and an impressive low detection limit which is lower than the limit of CN^- in drinking water (0.2 ppm) set by the United States Environmental Protection Agency (EPA). Another advantageous feature of cyanide probe, i.e., ratiometric response in the optical spectrum, can be acquired by an ICT redirection process in probe **2**, which will be discussed in the following section.

3.3. Optical Response of Probe 2 toward Cyanide Anion. Different from probe **1**, the absorption spectra of probe **2** showed four main absorption bands centering at 570, 452, 360, and 293 nm, respectively (Figure 6). Upon addition of CN^-, both absorption bands at 570 and 452 nm gradually decreased. Another decrease in the absorbance at 360 nm was also observed with a concomitant bathochromic shift of 10 nm. Furthermore, a remarkable increase in the intensity of absorption occurred at 293 nm. The well-defined isosbestic

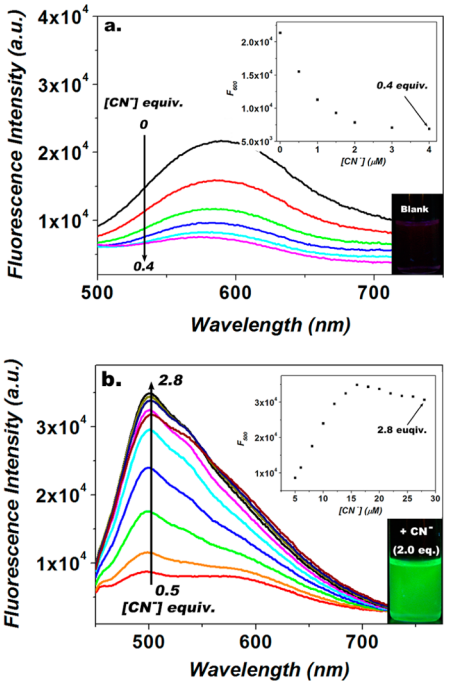

Figure 5. Fluorescence emission spectra of **1** (10 μM) in CH_3CN with titration of aqueous cyanide anion upon excitation at 400 nm. (a) Addition of 0–0.4 equiv of cyanide. (inset) Change of fluorescence intensity at 600 nm. (b) Addition of 0.5–2.8 equiv. (inset) Change of fluorescence intensity at 500 nm. Photographic images: the fluorescence image in the absence (inset a) and presence (inset b) of cyanide under a UV lamp at 365 nm.

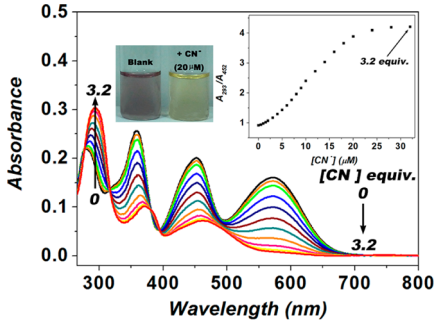

Figure 6. UV–vis spectra of probe **2** (10 μM) in CH_3CN upon addition of CN^- (0–32 μM). Each spectrum was obtained after addition of cyanide at 25 °C for 2 min. (inset) Absorbance intensity ratio of A_{293}/A_{452} upon addition of CN^- (right); photographic image of **2** before and after addition of 2.0 equiv CN^- (left).

point at 316 nm indicates the formation of the $[\mathbf{2}–CN]^-$ adduct. The solution of probe **2** changed from dark brown to light yellow upon the addition of CN^-, which can be observed by the naked eye. An appealing ratiometric absorbance signal (at 293 and 452 nm) was achieved as shown in the inset of Figure 6. The maximal ratio signal representing the saturation point of reaction was achieved after 3.2 equiv of cyanide was added.

The change in fluorescent intensity of probe **2** upon titration with CN^- was recorded and shown in Figure 7. The free compound **2** exhibited a near-infrared maximum emission peak at 720 nm, showing a 10 nm hypsochromic shift compared to that of probe **1**. Upon addition of CN^- the fluorescence intensity at 720 nm sharply decreased, accompanied by the

dx.doi.org/10.1021/am303152w | ACS Appl. Mater. Interfaces 2013, 5, 1317–1326

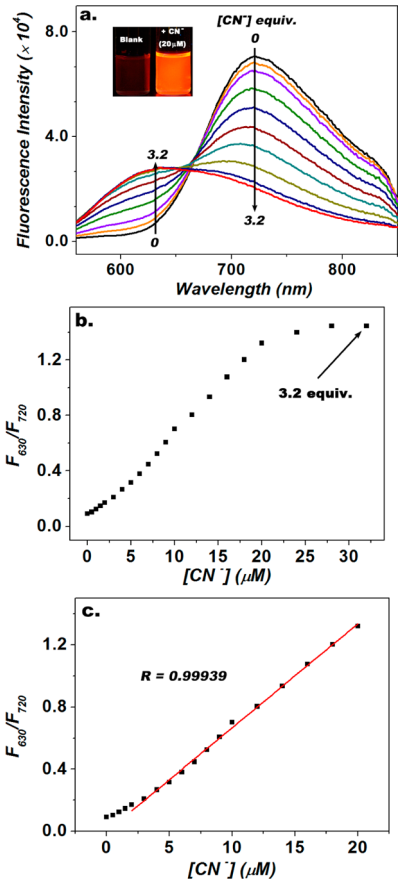

Figure 7. (a) Fluorescence spectra of **2** (10 μM) in CH_3CN upon addition of CN^- (0−32 μM). (inset) Fluorescence image in the absence and presence of cyanide under a UV lamp at 365 nm. (b) Plot of fluorescence intensity ratio (F_{630}/F_{720}) of **2** (10 μM) upon addition of CN^- (0−32 μM). λ_{ex} = 540 nm. Slits: 10 nm/10 nm. (c) Fluorescence intensity ratio (F_{630}/F_{720}) as a linear function of CN^- concentration from 0−18 μM.

occurrence of a new fluorescent emission band at 630 nm. An isoemissive point was clearly identified at 664 nm, suggesting the development of a new fluorophore. The color of fluorescence changed from dark red to orange and could be detected by the naked eye (Figure 7a inset). The ratiometric fluorescence intensity signal at 630 and 720 nm became constant when the amount of CN^- in the system reached 3.2 equiv (Figure 7b).

The detection limit of probe **2** was determined to be 2.31 × 10^{-8} M (see Figure 7c and Figure S19 in page S13, Supporting Information), which is lower than that of probe **1** and also below the maximum contaminant level (MCL) for cyanide in drinking water (0.2 ppm) set by the United States Environmental Protection Agency.

3.4. ^{1}H NMR and HRMS Titration. To investigate the reaction processes of the probes, we monitored the ^{1}H NMR spectral changes of probes **1** and **2** upon 0−2.1 or 0−1.0 equiv of cyanide anion in CH_2Cl_2 (to avoid the interference of 7.26 ppm solvent peak of $CDCl_3$). The reaction route was shown in Scheme 1.

*3.4.1. ^{1}H NMR and HRMS Titration of Probe **1**.* As a result of two reactive dicyano-vinyl groups respectively attached to each side, the ^{1}H NMR spectral change of probe **1** is more complicated than that of probe **2**. After addition of 2.1 equiv of cyanide anions, the peaks of the resonance α-H corresponding to the vinylic proton (H_c and H_d) at 7.31 ppm completely disappeared while a new peak grew up at 4.12 ppm corresponding to the reaction product tricyano-ethyl proton (H_c'' and H_d''). Meanwhile, the aromatic protons (H_e'', H_g'', H_i'') of dihydrophenazine core exhibited anticipated upfield-shift due to the sharply decreased electron withdrawing effect of dicyano-vinyl groups (Figure 8), illustrating the formation of

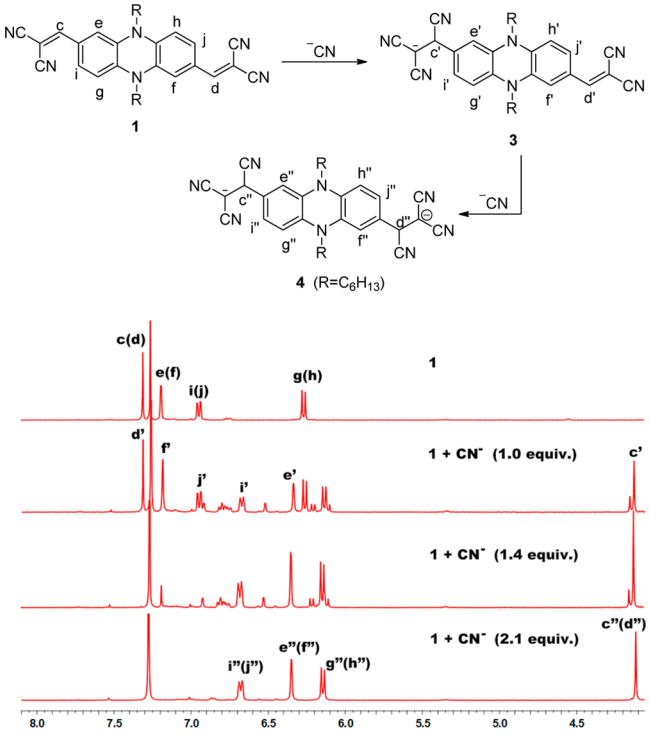

Figure 8. ^{1}H NMR titration spectroscopy of probe **1** in $CDCl_3$ (20.0 mM) upon addition of cyanide anion (as tetrabutylammonium salts in CH_2Cl_2) at 25 °C.

compound **4** which was confirmed by the peak at m/z = 554.2902 (calcd = 554.2906) corresponding to $[CN-\mathbf{1}-CN]^{2-}$ in HRMS analysis (Supporting Information Figure S16). Furthermore, when 1.0 equiv of cyanide anion was added, the approximate 1:1 integral ratio of H_e' and H_f' (same as the ratio of H_g' and H_h' and that of H_i' and H_j') indicated the formation of compound **3** (Supporting Information Figure S15). These consequences together with the HRMS peaks at m/z = 528.2874 (calc = 528.2876) corresponding to $[\mathbf{1}-CN]^-$ and m/z = 554.2902 (calc = 554.2906) corresponding to $[CN-\mathbf{1}-CN]^{2-}$ further supported our prediction of the step-by-step reaction procedure (Supporting Information Figure S16).

*3.4.2.. ^{1}H NMR and HRMS Titration of Probe **2**.* Probe **2** has only one dicyano-vinyl group. After the addition of 1.0 equiv of cyanide, the α-proton (H_a) at 7.96 ppm completely vanished, while a new signal (H_a') contemporarily appeared at 4.28 ppm (Figure 9). Such a drastic upfield shift of the vinyl α-H suggests the breaking of the C=C double bond and the formation of the new C−C single bond between cyanide and α-C of the dicyano-vinyl during nucleophilic addition reaction. Besides, another ^{1}H NMR upfield shift from 9.61 ppm (H_b) to 9.54 ppm (H_b') was observed, corresponding to the α-proton of the formyl group. Specifically, when 0.5 equiv of cyanide was added, the four equally integral signals (H_a, H_a', H_b, and H_b') further revealed the 1:1 reaction ratio between **2** and cyanide.

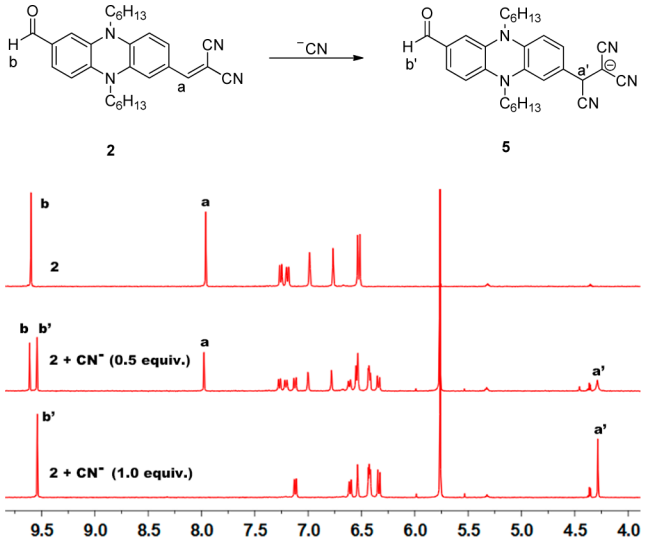

Figure 9. ^{1}H NMR titration spectroscopy of probe **2** in DMSO-d_6 (20.0 mM) upon addition of cyanide anion (as tetrabutylammonium salts in CH_2Cl_2) at 25 °C.

Further evidence for the 1:1 adduct of **2** and cyanide was found in HRMS spectroscopy analysis, in which the peak at m/z = 480.2754 (calc = 480.2763) corresponding to $[\mathbf{2}-CN]^-$ was clearly observed (Supporting Information Figure S17).

3.5. Theoretical Calculations. To gain further insight into the cyanide-sensing mechanism of probes **1** and **2**, density functional theory (DFT) calculations were carried out at the B3LYP/6-31G* level of theory.

The results of probe **1** are summarized in Supporting Information Tables S1 and S2 which show good agreement with experimental measurements. The absorbance at around 370 nm arises mainly from the dihydropheazine core. Upon chemical reaction with one CN^- anion, the asymmetric $[\mathbf{1}-CN]^-$ adduct was formed, resulting in an allowed highest occupied molecular orbital (HOMO) → lowest unoccupied molecular orbital (LUMO) transition corresponding to ICT from dihydropheazine core to the remaining dicyano-vinyl group (Figure 10 and Supporting Information Tables S3 and S4). This ICT absorption band is located at around 600 nm and has an oscillator strength smaller than that of **1** (Figure 10); therefore, the initial addition of CN^- anion leads to a bathochromic shift in absorption wavelength and a decrease in absorbance, in agreement with experimental measurements. Further chemical reaction of $[\mathbf{1}-CN]^-$ with CN^- gave rise to the $[CN-\mathbf{1}-CN]^{2-}$ adduct, and the ICT absorption band disappeared due to the destruction of the dicyano-vinyl groups.

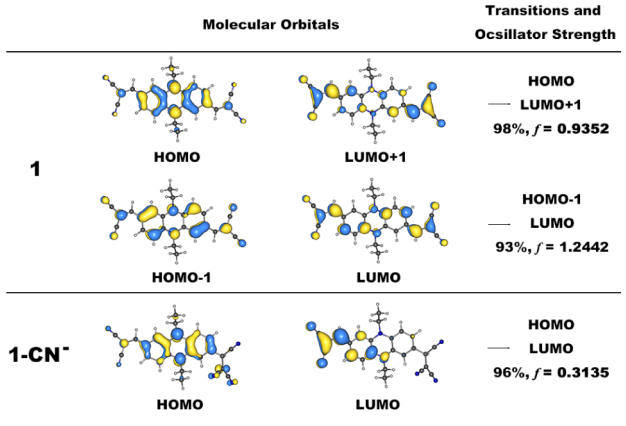

Figure 10. Calculated frontier molecular orbitals of probe **1** and the $[\mathbf{1}-CN]^-$ adduct.

Computed geometrical relaxation of the singlet first excited state (S1) of probe **1** suggests an $S_1 \rightarrow S_0$ emission at 687 nm with an oscillator strength of zero (Supporting Information Table S7); however, the intensity of $S_1 \rightarrow S_0$ emission can be acquired through Herzberg–Teller (HT) coupling with the closely positioned S_2 state which has a large oscillator strength of 1.2801, thus explaining the origination of experimentally observed luminescence at around 730 nm. This mechanism has been suggested to be present in dihydropheazine compounds.[55] Besides, the very close energy levels of S_1 and S_2 ($\Delta E \approx 20$ kJ/mol) could possibly give rise to $S_2 \rightarrow S_0$ emission at 606 nm (Table S8) from thermally populated S_2 state,[56] corresponding to the observed luminescence at 600 nm upon excitation at 400 nm. When a large concentration of CN^- anion has been added, formation of $[CN-\mathbf{1}-CN]^{2-}$ leads to the elimination of luminescence at 600 nm and appearance of luminescence at around 500 nm (Supporting Information Table S9), corresponding to typical fluorescence of dihydropheazine moiety.

As shown in Figure 11 and Supporting Information Table S11, the π-type HOMO of probe **2** is delocalized on the central

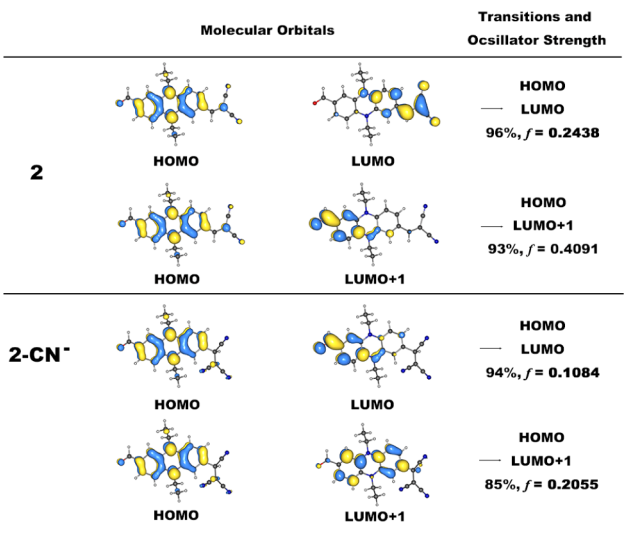

Figure 11. Calculated frontier molecular orbitals of probe **2** and $[\mathbf{2}-CN]^-$ adduct.

dihexyldihydrophenazine unit with extensions onto the formyl and dicyano-vinyl groups. The π^*-type LUMO and LUMO + 1 are mainly localized on the dicyano-vinyl and formyl groups, respectively. Time-dependent density functional theory (TDDFT) calculations revealed that photoinduced ICT could occur from phenazine to these two electron-withdrawing groups, resulting in two different ICT absorption bands at 570 and 450 nm corresponding to HOMO → LUMO and HOMO → LUMO + 1 transitions, respectively. Upon addition of CN^-, the dicyano-vinyl double bond was broken by nucleophilic attack of cyanide; the energy levels of HOMO was lifted due to diminished π-conjugation (Supporting Information Table S13), and the LUMO became localized on the formyl group with partial contribution from the phenazine core, which is in similar shape to LUMO + 1 of **2**. Therefore, in the $[\mathbf{2}-CN]^-$ adduct, the HOMO → LUMO transition corresponds to ICT from phenazine core to formyl group

dx.doi.org/10.1021/am303152w | ACS Appl. Mater. Interfaces 2013, 5, 1317–1326

(~450 nm), while a HOMO → LUMO + 1 transition corresponds to the absorption band of the phenazine core located at around 370 nm.

Geometrical relaxation and fluorescent decay of the singlet first excited state (S_1), which are of great importance in explaining the ratiometric fluorescent spectra of probe **2** upon addition of cyanide anion, were also studied by TDDFT calculations. It is found that the geometry of **2** at a relaxed S_1 state showed an elongation of the vinyl C=C double bond due to the π^* nature of its LUMO (Supporting Information Table S14), which is largely contributed by the dicyano-vinyl group. Such a geometrical change resulted in an increased HOMO energy level and a decreased LUMO energy level, therefore narrowing the HOMO−LUMO energy gap and leading to a large Stokes shift. The computed fluorescent wavelength from relaxed S_1 state is 720 nm, in good agreement with experimental spectrum (~720 nm, Figure 7 and Supporting Information Table S14). We also obtained the radiative rate constant of 4.6×10^7 s^{-1} for the fluorescent process of probe **2** from the working equation $k_r = 0.667f\bar{\nu}^2$, where f is oscillator strength and $\bar{\nu}$ is the wavenumber of emission (inverse centimeters). This theoretical prediction is quite close to the experimentally measured k_r, 2.8×10^7 s^{-1}, obtained as φ_{em}/τ where φ_{em} is quantum yield of fluorescence (0.08) and τ is measured lifetime (2.82 ns), confirming the rationality and reliability of theoretical calculations. Differently, the $[\mathbf{2}-CN]^-$ adduct has its LUMO mainly localized on the formyl group (Figure 11); at relaxed S_1 state the C=O double bond in the formyl group of $[\mathbf{2}-CN]^-$ adduct was elongated, resulting in a narrowed HOMO−LUMO gap and a Stokes shift similar to **2** (Supporting Information Table S15). The computed fluorescent wavelength of $[\mathbf{2}-CN]^-$ adduct is 591 nm, comparable to the experimentally measured result (~630 nm). Furthermore, the computed oscillator strength values for the $S_1 \rightarrow S_0$ fluorescence of probe **2** and $[\mathbf{2}-CN]^-$ adduct are 0.3566 and 0.1399, respectively, and their ratio (ca. 2.5:1) is in quantitative agreement with the ratio between the maximal emission intensities before and after the addition of cyanide anions (Figure 7a).

The ICT characteristics of fluorescence from the excited state of **2** and $[\mathbf{2}-CN]^-$ were also confirmed by measuring the solvatochromic behavior of emission spectra in three different solvents, namely toluene, dichloromethane, and acetonitrile. As shown in Figure 12, the wavenumber of fluorescent emission was plotted against the polarity parameter defined as $(\varepsilon - 1)/(2\varepsilon + 1) - (n^2 - 1)/(4n^2 + 2)$, where ε and n are dielectric constant and refractive index of the solvent, respectively. Both data sets for **2** and $[\mathbf{2}-CN]^-$ show very nice linear correlation. From the slope of the fitted line, it is estimated[57] that the dipole moment of the excited state of **2** and $[\mathbf{2}-CN]^-$ are 11.08 and 10.95 D, respectively. For comparison, the computed ground state dipole moment of **2** and $[\mathbf{2}-CN]^-$ are 6.75 and 20.15 D, respectively, the latter being very large due to its anionic character. The dramatic changes in dipole moments of **2** and $[\mathbf{2}-CN]^-$ from ground state to excited state strongly support the ICT nature of their fluorescent emission. Besides, TDDFT calculations reveal that the dipole moment of the excited state in acetonitrile are 18.87 and 15.97 D for **2** and $[\mathbf{2}-CN]^-$, respectively, suggesting that the dipole moment is amplified by the presence of highly polar solvent.

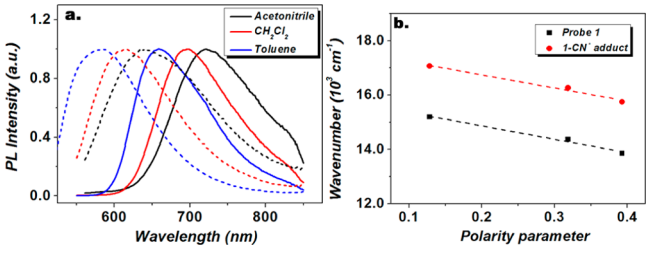

Figure 12. (left) Solvatochromism of emission spectra of (full line) **2** and (dotted line) $[\mathbf{2}-CN]^-$. (right) Dependence of emission wavenumber on polarity parameter of solvent.

3.6. Selectivity and Anti-interference Ability. High selectivity and anti-interference ability are important features for a chemodosimeter. To evaluate the selectivity of probes **1** and **2** for cyanide detection, the changes in absorption and fluorescence spectra (both in CH_3CN, 10 μM at 25 °C) caused by CN^- (20 μM) and miscellaneous interference anions (200 μM) including F^-, Cl^-, Br^-, I^-, PO_4^{3-}, CO_3^{2-}, SO_4^{2-}, NO_3^-, SCN^-, AcO^-, HSO_3^-, NO_2^-, and HCO_3^- with their Na^+ or K^+ salts in aqueous solutions were recorded. As a consequence of its two reactive units and stronger reactivity, probe **1** showed a visible disturbance by the interference species in high equivalents (Supporting Information Figure S20). However, these interferences are negligible compared to the response signal against cyanide anion. As can be seen, due to the advantage of ratiometric response, these interference anions did not cause probe **2** any significant colorimetric or ratiometric change in either absorption or fluorescence emission spectra. Moreover, in the presence of various interference species, the CN^- still caused similar ratiometric absorption and fluorescence intensity signals of probe **2** (Figure 13). In our experiment, acetonitrile was employed as the solvent, which is fully miscible with water. We explored optical response of the probes upon gradual addition of aqueous solution of CN^- and/or miscellaneous interference anions. Our experimental results together with theoretical interpretations indicate that the two

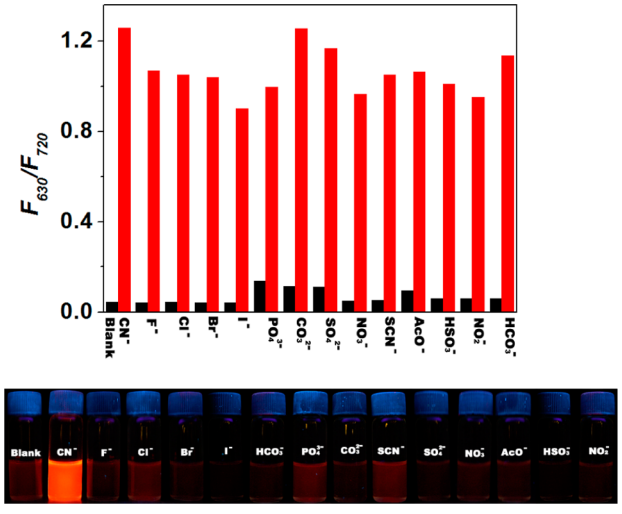

Figure 13. (above) Fluorescence intensity changes (F_{630}/F_{720}) of **2** (10 μM in CH_3CN) upon addition of 2 equiv of CN^- (in its tertbutylammonium water solution) and 20 equiv of various interference anions. Black bars represent the responses of **2** to the anions of interest. Red bars represent the subsequent additioin of 2 equiv (20 μM) of CN^-. (below) Visible fluorescence responses of probe **2** (10 μM in CH_3CN) in the presence of various other anions (20 equiv) in water under a UV lamp at 365 nm.

probes reported in our manuscript are fully capable of sensing aqueous CN^- ions even in the presence of interference anions. Therefore, limited water solubility of organic sensors does not prohibit their applicability; by mixing a certain volume of water sample with acetonitrile solution of our probe we will be able to determine the amount of cyanide ions in the sample from the colorimetric and ratiomatric sensing signals of the probe.

4. CONCLUSIONS

In summary, we have developed two alkyl-substituted phenazine derivative based chemodosimeters for cyanide, namely **1** and **2**. Both of them can be used as a highly selective and sensitive probe for detecting nanomolar levels of CN^-. Probe **1**, with two dicyano-vinyl groups as the reactive site, demonstrated a characteristic two-step reaction mechanism. An on−off NIR fluorescence emission change of 730 nm provided a remarkable detection limit of 5.77×10^{-8} M. The dramatic color change from deep purple to colorless enabled detection by the naked eye. In particular, probe **2** carrying a formyl group and a dicyano-vinyl group, exhibited an impressive ratiometric NIR response at 720 and 630 nm upon addition of aqueous cyanide anion, thus giving a more sensitive chemodosimeter with highly selectivity and lower detection limit of 2.31×10^{-8} M. ^{1}H NMR, HRMS characterizations, DFT, and TDDFT calculations confirmed that the sensing ability of **2** originated from the "A−D−A" → "A−D−D" structural change that leads to a redirection of ICT channels for absorption and fluorescence. Compared to many other fluorophores, the relatively uncomplicated synthesis and ratiometric NIR fluorescence response make the phenazine chemodosimeter a promising precursor and sensing platform for the development of other reactive dual-modal cyanide detection.

■ ASSOCIATED CONTENT

Ⓢ Supporting Information

Experimental procedures in detail, structural proofs, additional spectral data for probes **1** and **2**, and other new compounds. This material is available free of charge via the Internet at http://pubs.acs.org.

■ AUTHOR INFORMATION

Corresponding Author

*E-mail: jlhua@ecust.edu.cn. Fax: 86-21-64252758. Tel.: 86-21-64250940.

Author Contributions

[§]These authors contributed equally to this work.

Notes

The authors declare no competing financial interest.

■ ACKNOWLEDGMENTS

This work was supported by NSFC/China (2116110444 and 21172073), the National Basic Research 973 Program (2013CB733700), the Fundamental Research Funds for the Central Universities (WJ0913001). J.-L.H. appreciates Prof. H. Tian very much for his helpful discussion and valuable comments.

■ REFERENCES

(1) Boening, D. W.; Chew, C. M. *Water, Air, Soil Pollut.* **1999**, *109*, 67−79.
(2) Xu, Z. C.; Chen, X. Q.; Kim, H. N.; Yoon, J. Y. *Chem. Soc. Rev.* **2010**, *39*, 127−137.
(3) Jiang, J. Z.; Wang, X. Y.; Zhou, W. J.; Gao, H. C.; Wu, J. G. *Phys. Chem. Chem. Phys.* **2002**, *4*, 4489−4494.
(4) Gerberding, J. L. *Toxicological Profile for Cyanide*; U.S. Department of Health and Human Services: Atlanta, 2006.
(5) Pritchard, J. D. *Hydrogen Cyanide Toxicological Overview*; Health Protection Agency: U. K., 2007.
(6) Lou, X. D.; Ou, D. X.; Li, Q. Q.; Li, Z. *Chem. Commun.* **2012**, *48*, 8462−8477.
(7) Lindsay, A. E.; Greenbaum, A. R.; O'Hare, D. *Anal. Chim. Acta* **2004**, *511*, 185−195.
(8) Casella, I. G.; Gatta, M. *Electroanalysis* **2001**, *13*, 549−554.
(9) Lou, X. D.; Qiang, L.; Qin, J. G.; Li, Z. *ACS Appl. Mater. Interfaces* **2009**, *1*, 2529−2535.
(10) Lou, X. D.; Zhang, L. Y.; Qin, J. G.; Li, Z. *Chem. Commun.* **2008**, *44*, 5848−5850.
(11) Zou, Q.; Li, X.; Zhang, J. J.; Zhou, J.; Sun, B. B.; Tian, H. *Chem. Commun.* **2012**, *48*, 2095−2097.
(12) Yang, Y.; Zhao, Q.; Feng, W.; Li, F. Y. *Chem. Rev.* **2012**, *113*, 192−270.
(13) Li, Z. A.; Lou, X. D.; Yu, H. B.; Li, Z.; Qin, J. G. *Macromolecules* **2008**, *41*, 7433−7439.
(14) Lou, X. D.; Zeng, Q.; Zhang, Y.; Wan, Z. M.; Qin, J. G.; Li, Z. *J. Mater. Chem.* **2012**, *22*, 5581−5586.
(15) Lou, X. D.; Qiang, L.; Qin, J. G.; Li, Z. *ACS Appl. Mater. Interfaces* **2012**, *4*, 2133−2138.
(16) Lou, X. D.; Zhang, Y.; Qin, J. G.; Li, Z. *Chem. —Eur. J.* **2011**, *17*, 9691−9696.
(17) Kim, G. J.; Kim, H. J. *Tetrahedron Lett.* **2010**, *51*, 185−187.
(18) Park, S.; Kim, H. J. *Sens. Actuators, B* **2012**, *161*, 317−321.
(19) Pard, S.; Kim, H. J. *Sens. Actuators, B* **2012**, *168*, 376−380.
(20) Lv, X.; Liu, J.; Liu, Y.; Zhao, Y.; Sun, Y. Q.; Wang, P.; Guo, W. *Chem. Commun.* **2011**, *47*, 12843−12845.
(21) Lee, K. S.; Kim, H. J.; Kim, G. H.; Shin, I.; Hong, J. I. *Org. Lett.* **2008**, *10*, 49−51.
(22) Jung, H. S.; Han, J. H.; Kim, Z. H.; Kang, C.; Kim, J. S. *Org. Lett.* **2011**, *13*, 5056−5059.
(23) Yuan, L.; Lin, W.; Yang, Y.; Song, J.; Wang, J. *Org. Lett.* **2011**, *13*, 3730−3733.
(24) Lee, J. H.; Jeong, A. R.; Shin, I. S.; Kim, H. J.; Hong, J. I. *Org. Lett.* **2010**, *12*, 764−767.
(25) Cheng, X. H.; Tang, R. L.; Jia, H. Z.; Feng, J.; Qin, J. G.; Li, Z. *ACS Appl. Mater. Interfaces* **2012**, *4*, 4387−4392.
(26) Hong, S. J.; Yoo, J.; Kim, S. H.; Kim, J. S.; Yoon, J. Y.; Lee, C. H. *Chem. Commun.* **2009**, *45*, 189−191.
(27) Kim, S. H.; Hong, S. J.; Yoo, J.; Kim, S. K.; Sessler, J. L.; Lee, C. H. *Org. Lett.* **2009**, *11*, 3626−3629.
(28) Guliyev, R.; Ozturk, S.; Sahin, E.; Akkaya, E. U. *Org. Lett.* **2012**, *14*, 1528−1531.
(29) Lee, C. H.; Yoon, H. J.; Shim, J. S.; Jang, W. D. *Chem.—Eur. J.* **2012**, *18*, 4513−4516.
(30) Guliyev, R.; Buyukcakir, O.; Sozmen, F.; Bozdemir, O. A. *Tetrahedron Lett.* **2009**, *50*, 5139−5141.
(31) Liu, Z.; Wang, X.; Yang, Z.; He, W. *J. Org. Chem.* **2011**, *76*, 10286−10290.
(32) Tsui, Y. K.; Devaraj, S.; Yen, Y. P. *Sens. Actuators, B* **2012**, *161*, 510−519.
(33) Niu, H. T.; Jiang, X.; He, J.; Cheng, J. P. *Tetrahedron Lett.* **2009**, *50*, 6668−6671.
(34) Liu, J. L.; Liu, Y.; Liu, Q.; Li, C. Y.; Sun, L. N.; Li, F. Y. *J. Am. Chem. Soc.* **2011**, *133*, 15276−15279.
(35) Kim, Y.; Huh, H. S.; Lee, M. H.; Lenov, I. L.; Zhao, H.; Gabbai, F. P. *Chem.—Eur. J.* **2011**, *17*, 2057−2062.
(36) Hudnall, T. W.; Gabbai, F. P. *J. Am. Chem. Soc.* **2007**, *129*, 11978−11986.
(37) Badugu, R.; Lakowicz, J. R.; Geddes, C. D. *J. Am. Chem. Soc.* **2005**, *127*, 3635−3641.
(38) Nolan, E. M.; Lippard, S. J. *Chem. Rev.* **2008**, *108*, 3443−3480.
(39) Peng, X. J.; Wu, Y. K.; Fan, J. L.; Tian, M. Z.; Han, K. *J. Org. Chem.* **2005**, *70*, 10524−10531.

(40) Qu, Y.; Hua, J. L.; Tian, H. *Org. Lett.* **2010**, *12*, 3320−3323.
(41) Yao, L. M.; Zhou, J.; Liu, J. L.; Feng, W.; Li, F. Y. *Adv. Funct. Mater.* **2012**, *22*, 2667−2672.
(42) Li, C. Y.; Yu, M. X.; Sun, Y.; Wu, Y. Q.; Huang, C. H.; Li, F. Y. *J. Am. Chem. Soc.* **2011**, *133*, 11231−11239.
(43) Huang, X. M.; Guo, Z. Q.; Zhu, W. H.; Xie, Y. S.; Tian, H. *Chem. Commun.* **2008**, *44*, 5143−5145.
(44) Hiraoka, S.; Okamoto, T.; Kozaki, M.; Shiomi, D.; Sato, K.; Takui, T.; Okada, K. *J. Am. Chem. Soc.* **2004**, *126*, 58−59.
(45) Terada, E.; Okamoto, T.; Kozaki, M.; Masaki, M. E.; Shiomi, D.; Sato, K.; Takui, T.; Okada, K. *J. Org. Chem.* **2005**, *70*, 10073−10081.
(46) Thalladi, V. R.; Smolka, T.; Gehrke, A.; Boese, R.; Sustmann, R. *New J. Chem.* **2000**, *24*, 143−147.
(47) Frisch, M. J.; Trucks, G. W.; Schlegel, H. B.; Scuseria, G. E.; Robb, M. A.; Cheeseman, J. R.; Scalmani, G.; Barone, V.; Mennucci, B.; Petersson, G. A.; et al. *Gaussian 09*, revision A.2; Gaussian, Inc.: Wallingford CT, 2009.
(48) Becke, A. D. *J. Chem. Phys.* **1993**, *98*, 5648−5652.
(49) Hehre, W. J.; Ditchfield, R.; Pople, J. A. *J. Chem. Phys.* **1972**, *56*, 2257−2261.
(50) Tomasi, J.; Mennucci, B.; Cammi, R. *Chem. Rev.* **2005**, *105*, 2999−3093.
(51) Perdew, J. P.; Burke, K.; Ernzerhof, M. *Phys. Rev. Lett.* **1996**, *77*, 3865−3868.
(52) Leang, S. S.; Zahariev, F.; Gordon, M. S. *J. Chem. Phys.* **2012**, *136*, 104101−12.
(53) Hong, S. J.; Yoo, J.; Kim, S. H.; Kim, J. S.; Yoon, J.; Lee, C. H. *Chem. Commun.* **2009**, *45*, 189−191.
(54) Ding, Y. B.; Xie, Y. S.; Li, X.; Hill, J. P.; Zhang, W. B.; Zhu, W. H. *Chem. Commun.* **2011**, *47*, 5431−5433.
(55) Bunsenges, B. *Phys. Chem.* **1974**, *78*, 1348−1353.
(56) Turro, N. J.; Ramamurthy, V.; Cherry, W.; Farneth, W. *Chem. Rev.* **1978**, *78*, 125−145.
(57) Pasman, P.; Rob, F.; Verhoeven, J. W. *J. Am. Chem. Soc.* **1982**, *104*, 5127−5133.